

Indium nanodeposits: A substrate for metal-enhanced fluorescence in the ultraviolet spectral region

Anatoliy I. Dragan¹ and Chris D. Geddes^{2,a)}

¹*Institute of Fluorescence, University of Maryland, Baltimore County, 701 East Pratt Street, Baltimore, Maryland 21202, USA*

²*Institute of Fluorescence and Department of Chemistry and Biochemistry, University of Maryland, Baltimore County, 701 East Pratt Street, Baltimore, Maryland 21202, USA*

(Received 19 July 2010; accepted 14 September 2010; published online 3 November 2010)

We have studied a metallic substrate, composed of indium nanodeposits, for metal-enhanced fluorescence (MEF) in the ultraviolet (UV) spectral region. Indium coated slides were prepared using the thermal vapor deposition technique. Theoretical finite difference time domain simulations and experimental studies show that plasmon enhanced absorption and coupled radiation through the scattering component of the extinction spectra of indium nanoparticles, lie in UV region, and are sensitive to the size and density of the nanoparticles, the thickness of the indium film, and polarity of the medium. The MEF effect, measured for intrinsic protein tryptophan and tyrosine residues, loaded onto indium films of different thickness, changes in a wavelike fashion, reflecting changes in the metal film landscape and, consequently, the chromophores coupling with surface plasmons. Indium films also significantly enhance intrinsic fluorescence of proteins themselves [bovine serum albumin]. In this case the wavelength dependence of MEF shows different emission enhancements of protein Tyr and Trp residues. Subsequently, indium-enhanced intrinsic protein fluorescence in the UV spectral region can be of great potential importance for quantitation assays as well as for the labelless detection of biomolecules in the biosciences. © 2010 American Institute of Physics. [doi:10.1063/1.3503439]

I. INTRODUCTION

Fluorescence is a powerful technique for the detection of biological macromolecules (nucleic acids, proteins) *in vitro* and *in situ*, in the registration kinetics of multicomponent reactions, in molecular recognition, e.g., in immunoassays, and other biomedical approaches.¹ It utilizes both external fluorescent labels and probes, and internal (intrinsic) chromophores (tryptophan and tyrosine), which are naturally distributed throughout proteins. Persistent interest in the application of fluorescence methods to the biosciences has extensively stimulated the creation and synthesis of new highly luminescent external fluorescence probes, capable of specifically interacting with biomolecules by forming covalent and noncovalent bonds, recognizing specific substrates, covering a broad spectral range, from the ultraviolet (UV) to near infrared (NIR). Despite obvious progress in fluorescence based detection assays, there are still certain restraints in sensitivity, caused by limitations in brightness and the extinction of fluorophores, as well as their limited photostability. The recent introduction into practice of the metal-enhanced fluorescence (MEF) approach, which can dramatically [3–1000 fold, depending on the origin of a chromophore, geometry of the system, solvent polarity, kind of metal, size and density of nanoparticles (NPs), and, especially, proximity of a chromophore to the NP's surface] increase fluorescence intensity of chromophores in the far-field, has tremendously improved the sensitivity of fluorescence-based assays.^{2–5}

The MEF approach is based on the effect of coupling of a chromophore's electronic system with surface plasmons of a metal NP and, as a result, amplified emission of the coupled quanta.^{4,6,7} This emission is extremely bright with a shorter lifetime, which, as a consequence, makes fluorophores considerably more photostable. The MEF effect depends on many factors, especially on the metal substrate. Different metals produce different size and shape particles that thermally deposited, which have different plasmon resonance frequencies. The most popular metals to date have been gold and silver.^{2,7–12} These noble metals have plasmon resonance bands in the visible (VIS) region and effectively enhance fluorescence of dyes in the VIS-NIR spectral region.¹³ In our laboratories we have also investigated other substrates and have shown that tin,¹⁴ chromium,¹⁵ nickel,¹⁶ zinc,¹⁷ and copper¹⁸ also have quite pronounced MEF properties in the visible spectral region. It has also been shown that aluminum films can enhance fluorescence in the UV spectral range.¹⁹

Intrinsic protein fluorescence stands somewhat aside from the developments and progress in external fluorophore probes and labels. Sensitivity of fluorescence assays therefore based on intrinsic protein fluorescence are fundamentally limited to the quantum yields of Tyr and Trp residues and their extinctions, which are significantly lower than that for commonly used external dyes.¹ On the other hand, natural intrinsic chromophores are a part of proteins themselves and participate in maintaining protein structure and associated properties. The fluorescence of Tyr and Trp residues gives valuable information regarding a protein's conformation, protein-protein and protein-DNA interactions as well as

^{a)}Electronic mail: geddes@umbc.edu.

molecular recognition. However, in many cases the labeling of proteins with external fluorescent dyes is not effective and can change protein structure or block function and an ability to bind partners. Therefore, there is significant interest in the biosciences for the increased sensitivity of intrinsic protein fluorescence based assays, and the ability to study native proteins.

In this study we subsequently demonstrate a new substrate for MEF in the UV spectral region—indium (In). We show that indium films of different thickness enhance fluorescence of both fluorophores, Tyr and Trp. To further demonstrate the usefulness of our approach we show the enhanced luminescence of bovine serum albumin (BSA) from indium coated wells.

II. MATERIAL AND METHODS

A. Materials

N-acetyl-tryptophan-amid (NATA) and *N*-acetyl-tyrosine (NA-Tyr) were purchased from Sigma. The concentration of NATA and NA-Tyr were determined by measuring the optical density of the solutions using extinction coefficients of $E_{280}=5300 \text{ M}^{-1} \text{ cm}^{-1}$ and $E_{275}=1400 \text{ M}^{-1} \text{ cm}^{-1}$,^{20,21} respectively. BSA was purchased from Sigma. To determine the concentration of the protein in solutions, an extinction coefficient of $E_{280}=43\,824 \text{ M}^{-1} \text{ cm}^{-1}$ was used. Indium wire, 99% pure, for thermal vapor deposition onto glass slides was purchased from the Kurt J. Lesker Co., Material Group (Clairton, PA). NATA, NA-Tyr, and BSA were dissolved in TE buffer, pH 7.4.

Absorption spectra of the protein intrinsic chromophores and BSA were measured using a Varian Spectrophotometer in quartz B7 1 cm path-length cuvettes.

Fluorescence spectra of NATA, NA-Tyr, and BSA were recorded using a Cary Eclipse spectrofluorimeter (Varian, Inc., USA) at room temperature. The solutions were sandwiched between a quartz slide and a glass slide with deposited indium, and for the control sample containing no metal, between quartz/glass slides. The samples were excited at 280 nm and the fluorescence monitored over the wavelength range 290–450 nm.

B. Time-resolved fluorescence decay measurements

The fluorescence intensity decay functions of the NATA on indium slides of different thickness and on glass (MEF control sample) were measured using a TEMPRO FLUORESCENCE LIFETIME SYSTEM (Horiba Jobin Yvon, USA). The reference cell contained colloidal silica, SM-30 ludox solution, used as a control (zero lifetime). Measurements were performed at room temperature. Determination of NATA excited state lifetimes (τ_i) and corresponding amplitudes (A_i) were undertaken using the TEMPRO FLUORESCENCE LIFETIME SYSTEM software, decay analysis and graphical output software (DAS6). In general, when a fluorescence decay function exhibited more than one exponent the amplitude weighted fluorescence lifetime was calculated as follows:

$$\langle \tau \rangle = \sum_{i=1}^n A_i \times \tau_i, \quad (1)$$

where n is a number of fluorescence decay components in the total decay function.

C. Numerical finite difference time domain (FDTD) simulations

The two-dimensional (2D) computational simulation of the electric field intensities and near-field distributions at the surface of a 180 nm indium NP in a total field scattered field (TFSF) were undertaken using the FDTD method. TFSF sources are used to divide the computation area or volume into total field (incident plus scattered field) and scattered field only regions. The incident *p*-polarized electric field was defined as a plane wave with a wave-vector that is normal to the injection surface. Using FDTD SOLUTION software (Lumerical, Inc. <http://www.lumerical.com>), the simulation region was set to $550 \times 550 \text{ nm}^2$ with a mesh accuracy of 5. To minimize simulation times and maximize resolution of field enhancement regions around the particle arrangement, a mesh override region is set to 1 nm around the 180 nm NP. The overall simulation time was set to 50 fs and calculated over a broad wavelength range, using known permittivity values and refractive indices of indium. The wavelength dependence of the NP extinction, and cross-sections of its components, absorption and scattering, were calculated using LUMERICAL software script. To simulate effects of solvent polarity on plasmon resonance spectra, the background index was set to the corresponding refractive index of the respective solvent.

D. Thermal vapor deposition of indium

Thermal vapor deposition of indium onto glass slides was performed using an AUTO 306 Vacuum Coater instrument, equipped with SQM-160 Rate/Thickness Monitor (BOC Edwards, USA). Thickness of the deposited indium varied from 2 to 20 nm, as measured using the quartz-crystal microbalance. Real-color photographs of the indium slides, used in this study, are shown in Fig. 1.

E. Measurement of electrical resistance of metal-coated glass slides

Electrical resistance (conductivity) of indium and aluminum films was measured using a GTD-11 instrument (GB Instruments). The distance between flat-end electrodes, placed on the metal film, was 1 cm.

III. RESULTS AND DISCUSSION

A. Characterization of indium slides

Figure 1 shows indium slides, fabricated using thermal vapor deposition of the metal onto glass slides. As can be seen from Fig. 1, an increase in indium thickness progressively decreases the transparency of the slides, i.e., they become yellow-brownish. To characterize spectral properties of the slides in the UV spectral region, we additionally deposited indium on quartz slides. Figure 2 shows the optical den-

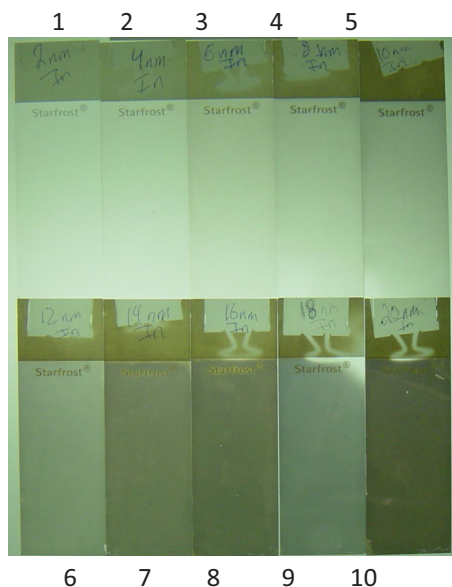


FIG. 1. (Color online) Indium slides fabricated using vacuum thermal vapor deposition of the metal onto a glass surface. Thickness of the indium films in slides Nos. 1–10 changes from ~ 2 to 20 nm, in 2 nm increments, respectively.

sity (absorbance) spectra of the indium films for 2 and 4 nm thicknesses. The maximum position of the plasmon resonance band is about 300 nm and the plasmon frequencies/absorption extends far into the VIS-NIR region. It is notable that a twofold increase in indium film thickness almost twice increases the optical density, without a change in the shape of the absorption band. It is known that the plasmon resonance band is dependent on the size of a NP and shifts to the red with an increased particle diameter.^{1,13} Therefore, we suggest that for low indium film thicknesses the size of deposited indium NPs is approximately the same. The conclusion reflects the vacuum coating process, i.e., metal deposits onto slides, the size of which is approximately the same; where they randomly coat the surface, forming a homogeneous but noncontinuous film on the glass slide.

Additional insight into the nature of the observed indium plasmon resonance band in the UV spectral region comes from numerical 2D FDTD simulations, which allow for the deconvolution of the extinction cross-section spectra into two components: absorption and scattering. The results of these simulations are shown in Fig. 3 (left). For the 180 nm NP the absorption cross-section approximately coincides

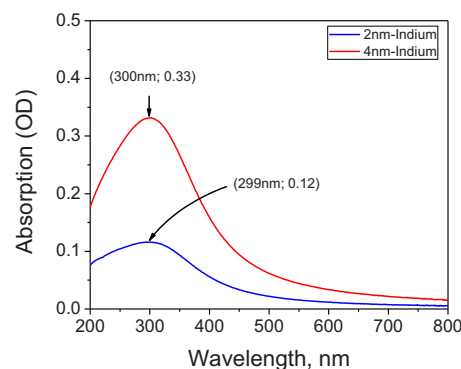


FIG. 2. (Color online) Plasmon absorption spectra of indium films deposited on quartz slides. Thickness of the films is 2 nm and 4 nm, respectively, as measured using the quartz crystal microbalance.

with the size of the particle. However, the scattering component of the extinction spectra has significantly greater cross-section, i.e., it is more dominant. Therefore, we can assume that the experimentally determined optical density spectra, which corresponds to the total, i.e., Extinction=Absorption + Scattering, spectra of NPs is determined mostly by the surface plasmon associated scattering component.

The position of the plasmon resonance spectra is sensitive to the refractive index (n) of the medium [Fig. 3 (left)]. Upon increase in n from 1.333 (water) to 1.5 (e.g., toluene) the spectra significantly shifts, almost 20 nm to the red. This shift is the effect of high-frequency polarizability of the solvent. This solvent relaxation effect or dipolar dephasing, decreases the energy of surface plasmon dipoles and causes a shift in the absorption spectra.

Coupling of the incident light with surface plasmons produces a strong E-field around the NP. Figure 3 (right) shows the distribution of the near-field around indium NPs upon irradiation with light, the wavelength of which corresponds to the maximum position of the extinction spectrum. The near-field distribution has specific character, it concentrates the field in certain positions on the surface, and enhances (concentrates) it nearly several orders of magnitude. This coupling of light with surface plasmons is a part of the MEF enhancement phenomenon.

Further increases in the thickness of the indium films results in further changes in their optical density spectra, and the appearance of a more pronounced yellow-brownish color. We have recorded the optical density of the indium glass

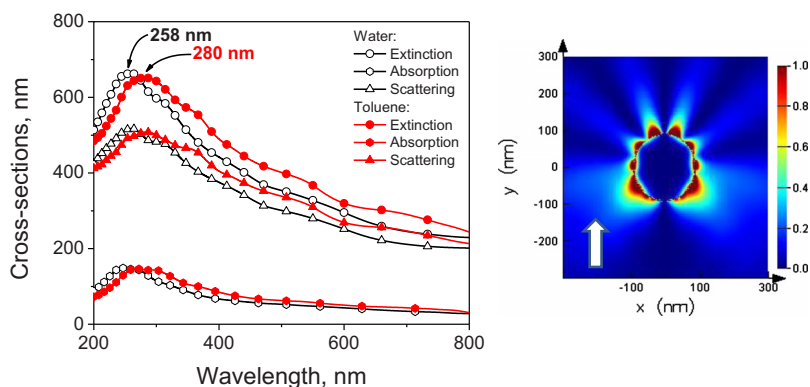


FIG. 3. (Color online) Left: extinction, absorption and scattering cross-section spectra of 180 nm In-NP in water ($n=1.333$) and toluene (1.496). Calculations were undertaken using FDTD simulations. Right: distribution of the near-field around the indium NPs upon irradiation with incident light at 270 nm. Arrow shows direction of incident light propagation in the simulations NP.

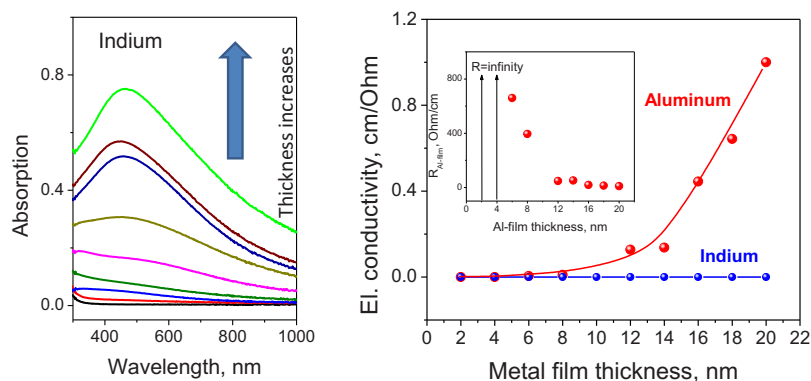


FIG. 4. (Color online) Left: absorption spectra of indium films deposited onto glass slides (cf. Fig. 1). Thickness of metal films varies from 2 nm to 20 nm, in 2 nm increments, respectively. Right: dependence of the electrical conductivity of indium and aluminum films on glass slides. Inset: dependence of the electrical resistance of aluminum films on glass slides.

slides in the wavelength range 300–1000 nm (Fig. 4). The plasmon resonance extinction band shifts to the visible region (redshift) and significantly increases in magnitude. The observed change in absorption spectra could be explained by saturation of the glass surface with NPs, formation of a semicontinuous indium film (at thicknesses >4 –6 nm) and then, upon further deposition, formation of larger islands on the metal surface. This dramatic change in indium surface landscape can lead to the appearance of the new broad plasmon resonance band with a maximum in the visible region, i.e., at about 450 nm. On the basis of the spectral data we can suggest that at high indium density, the surface consists of larger size particles or indeed touching smaller particles, but not a continuous thick layer. An additional argument, which supports this suggestion, comes from the results of electrical conductivity measurements. Indium slides, 2–20 nm thickness, are not conductive, i.e., even for thick 20 nm indium, the electrical resistance >2 M Ω /cm. In comparison, for aluminum slides, used as a control, we have observed (Fig. 4, right) an increase in conductivity starting from ~ 6 nm thickness, which progressively increases with metal density (for 20 nm aluminum slides the electrical resistance was about 10 Ω /cm).

In essence, the formation of the indium film surface landscape during vacuum deposition, is quite complex, but, looks likely to contain three discrete stages: (a) deposition of randomly distributed single NPs of nearly equal size (thickness between the 2 and ≥ 4 –6 nm) on glass; (b) saturation of the glass surface with NPs and the subsequent formation of a thin semicontinuous film; and (c) the merging NPs into large islands on the surface.

B. MEF of protein intrinsic chromophores

Fluorescence of NATA and NA-Tyr was studied using a simple sandwich geometry, i.e., by placing a protein solution between a quartz slide and an indium coated glass slide, the quartz/glass geometry being used as a control sample. A quartz slide was used on the excitation side since it is transparent to UV light, i.e., at the wavelength of excitation. The thickness of solution between the slides is ≈ 1 μm .²² The experimental geometry for the study of the MEF effect in the UV spectral region is shown in Fig. 5.

Figure 6 shows the results of MEF measurements undertaken for NATA and NA-Tyr, loaded onto indium slides of different thickness. Remarkably, both chromophores demon-

strate a similar, nonlinear, dependence of the MEF effect versus indium thickness. At low density the fluorescence enhancement almost linearly increases and reaches a maximum at a 4–6 nm thickness. A further increase in indium deposits on slides leads to a decrease in MEF. The minimum enhancement observed for both NATA and NA-Tyr fluorophores was at an indium film thickness of 10–12 nm, followed by a progressive increase in MEF, up to 20 nm thick. It is notable that, despite significant spectral difference between the chromophores, i.e., difference in extinction, quantum yield and in dipole moments,^{1,20,21,23} the trends in MEF dependence upon the thickness are very similar. Hence it is likely that the main factor, which underpins the fluorescence enhancement, is the indium film landscape itself. In fact, at low metal density (thickness <4 –6 nm), indium NPs are randomly distributed on the glass surface and a subsequent increase in thickness suggests an increase in density of separate NPs. MEF is a result of chromophore coupling with NP's surface plasmons¹³ and, one might at first expect that in this case the magnitude of fluorescence enhancement should linearly depend on the density of indium NPs (Fig. 6). However, the formation of a semicontinuous indium film (10–12 nm thickness) can significantly diminish MEF, as we have shown recently,²² due to NPs forming a metal film, and the lack of discrete plasmon confined resonances. Our laboratory has demonstrated this hypothesis for chemiluminescence solutions on both solid and particulate substrates.²⁴

The fluorescence enhancement of NATA and NA-Tyr for indium film thicknesses >12 nm is an interesting phenomenon, because it occurs after the formation of a thin but continuous coating. As it was discussed previously, vacuum

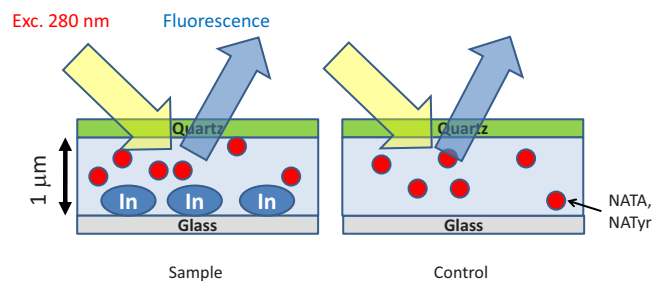


FIG. 5. (Color online) Experimental geometry for analysis of the MEF effect in the UV spectral region. Solutions of NATA (NATyr) loaded onto indium films. The “sandwich” sample geometry was used. Excitation and fluorescence spectra of tryptophan were monitored using a Varian Eclipse spectrofluorometer.

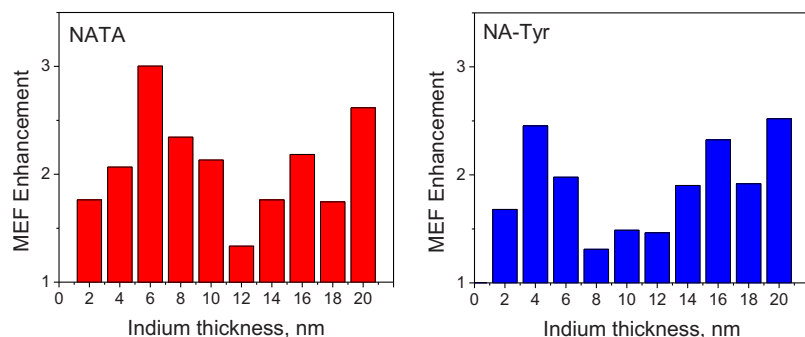


FIG. 6. (Color online) The MEF enhancement effect for NATA (left) and NATyr (right) observed on indium slides of different thickness. Measurements were undertaken in a sandwich geometry (see Fig. 5). Excitation at 270 nm.

deposition of indium on a metal surface forms particles (clusters), which have different plasmon properties and are characterized by a broad distribution of plasmon resonance frequencies, from the UV to the NIR spectral region (Fig. 4). Despite the difference in the nature of the plasmon resonance at high indium film thickness, as compared to low (2–4 nm) thickness, MEF increases almost linearly in this range, 12–20 nm.

We have also studied fluorescence intensity decay functions for NATA loaded onto indium slides. Figure 7 (left) shows a time-resolved fluorescence decay trace for NATA on glass. The decay is approaching monoexponential. The amplitude weighted lifetime [see Eq. (1)] of NATA in this control experiment is $\langle\tau\rangle=2.85\pm 0.004$ ns ($\chi^2=1.05$). In the presence of indium of different coating thicknesses, from 1 to 10 nm, the lifetime gradually decreases to $\langle\tau\rangle=2.44\pm 0.006$ ns ($\chi^2=1.10$), (Table I).

Presently, there are two mechanisms thought to drive fluorescence enhancement, i.e., MEF: radiation of an excited fluorophore through surface plasmon scattering modes and an enhanced excitation due to the intense E-field, associated with surface plasmons.^{4,13} The first mechanism results in an increase in the system (chromophore+NP) quantum yield and, in addition, it decreases the excited state lifetime due to a strong coupling of the electronic system of the fluorophore with surface plasmons, the fast plasmon lifetime reflecting the *coupled system lifetime*.² The second mechanism increases the excitation rate of the chromophore located within the intense near-field of the NP.^{4,13,15,17,25} Usually, for this mechanism alone, the excited state lifetime of the chromophore does not change, which has been observed for metals such as chromium.¹⁵ The results for NATA (Fig. 7 and

Table I) show that both mechanisms of NATA fluorescence enhancement are present, while the second mechanism, i.e., the electromagnetic near-field effect, is likely to be dominant.

C. Analysis of protein fluorescence enhancement on indium substrates

We also have studied MEF for BSA loaded onto indium slides. BSA is a large globular protein of molecular weight 69 323 Da, which contains 607 residues. There are 21 tyrosine and 3 tryptophan residues.²⁶ Despite a large content of tyrosines, the fluorescence spectrum of BSA is mostly underpinned by emission of the Trp chromophores, which invariably have higher quantum yields and extinction coefficients.^{20,21,23} Tyrosine chromophores have lower extinction coefficients²¹ and, in addition, a diminished emission particularly due to the effective quenching by other protein groups and energy migration to Trp's, when located within proteins.^{1,20,21}

Figure 8 shows the fluorescence spectra of BSA loaded onto a glass slide and indium 20 nm films. In the presence of indium, the fluorescence of BSA enhances \approx fourfold in the far-field. Considering that only 1% of solution is within the plasmon-enhancing range, one can assume that the net near-field enhancement might be about 100-fold greater, i.e., in total MEF \approx 400. Enhancement of BSA fluorescence, as it was shown for free Tyr and Trp chromophores, also depends on the indium coating thickness (Fig. 9). It should be noted that MEF for NATA does not depend on the wavelength of fluorescence but in the case of BSA, the fluorescence enhancement significantly depends on λ [Fig. 9 (right)], show-

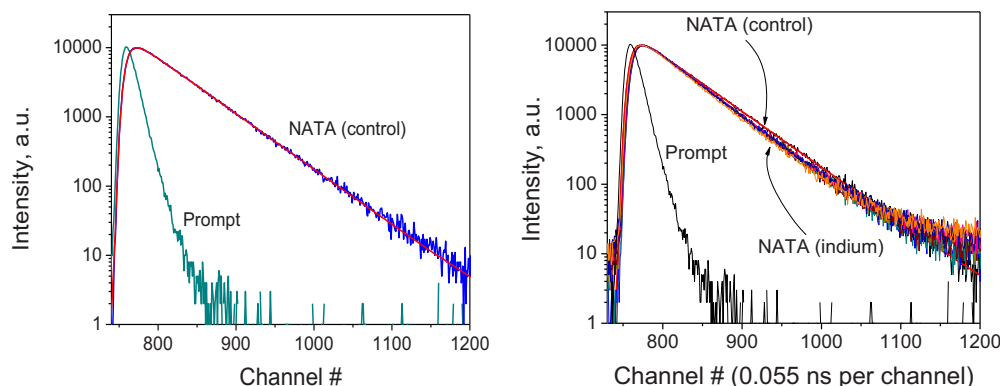


FIG. 7. (Color online) NATA time-resolved fluorescence intensity decay on glass (left) and on indium slides (right) (indium film thickness changes from 1 nm to 10 nm, in ~ 1 nm increments, respectively). Excitation was using a 282 nm pulsed light-emitting diode.

TABLE I. Fluorescence intensity decay parameters of NATA on glass (control sample) and on slides of different indium film thickness.

| Indium thickness (nm) | A_1 | τ_1 (ns) | A_2 | τ_2 (ns) | $\langle\tau\rangle^a$ (ns) | χ^2 |
|-----------------------|-------|------------------|-------|------------------|-----------------------------|----------|
| 0 (glass control) | 0.955 | 2.97 ± 0.004 | 0.045 | 0.25 ± 0.03 | 2.85 | 1.04 |
| 2 | 0.946 | 2.74 ± 0.006 | 0.054 | 0.38 ± 0.04 | 2.61 | 1.18 |
| 4 | 0.957 | 2.73 ± 0.004 | 0.043 | 0.24 ± 0.05 | 2.62 | 1.17 |
| 6 | 0.958 | 2.69 ± 0.006 | 0.042 | 0.39 ± 0.01 | 2.59 | 1.01 |
| 8 | 0.918 | 2.65 ± 0.007 | 0.082 | 0.116 ± 0.02 | 2.44 | 1.14 |
| 10 | 0.948 | 2.62 ± 0.006 | 0.052 | 0.29 ± 0.04 | 2.49 | 1.10 |

^a $\langle\tau\rangle$ is the amplitude weighted excited state lifetime of chromophores [see Eq. (1)].

ing a MEF increase from three to almost five in the 380 to 300 nm λ range. Interestingly, the observed change in MEF along with the wavelength of fluorescence is more pronounced at around 300 nm, where the fluorescence intensity of tyrosine is maximum. Subsequently, we suggest that the Tyr-component of the complex emission spectra of BSA, enhances sufficiently greater than the Trp-component.

We have analytically analyzed the complex fluorescence spectra of BSA, i.e., the contribution of Tyr and Trp fluorescence to the total emission spectra. To do this, we have fitted the fluorescence spectra of BSA, $S_{BSA}(280;\lambda)$, to the fluorescence spectra of tyrosine, $S_Y(280;\lambda)$, (it is known that the position of tyrosine emission is not sensitive to the polarity of microenvironment, i.e., the shape and position of Tyr-spectra is nearly constant^{1,20,21}) and to the fluorescence Trp-component of BSA. The Trp-component of BSA emission [$S_W(295;\lambda)$] was recorded using an excitation wavelength of 295 nm, where only Trp absorbs light.^{20,21,27} For the BSA spectra deconvolution we have used the following fitting equation:²⁷

$$S_{BSA}(280;\lambda) = A \times S_Y(280;\lambda) + B \times S_W(295;\lambda), \quad (2)$$

where A and B are the weighted amplitudes of tyrosine (Y) and tryptophan (W) fluorescence components.

The result of the BSA emission spectrum deconvolution is presented in Fig. 10. BSA fluorescence contains two components, tyrosine and tryptophan. The Tyr component weighted amplitude (at 304 nm, i.e., at the maximum of the Tyr fluorescence spectra) is about 13%. Upon loading on indium the Tyr- and Trp-components of the BSA fluorescence enhance differently, which is explained by the specific distribution of chromophores within the protein globule. This

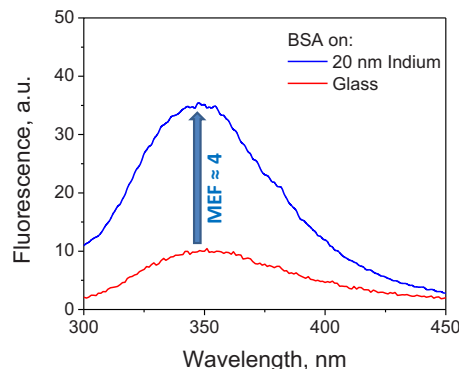


FIG. 8. (Color online) Fluorescence emission spectra of BSA loaded onto glass and indium films. Spectra were recorded on a Varian spectrofluorometer. Excitation was at ~ 280 nm. Solution of BSA was sandwiched between both quartz and indium coated glass.

distribution determines the effective distances between chromophores and the indium surface, i.e., modulates chromophore-plasmon coupling¹³ and, consequently, the magnitude of the MEF effect for each individual chromophore is likely to be different. A greater MEF effect for the Tyr chromophore is probably due to closer location to the surface of protein and, therefore, a shorter distance to the indium surface. Note, it is known that MEF is distance and wavelength dependent^{25,28,29} and occurs through space over a 0–30 nm distance.

Recently we have shown that the magnitude of MEF depends nonlinearly on incident light irradiation power³⁰ and results in an increased MEF of almost tenfold when the laser power is changed from 2 to 100 mW. This remarkable result gives one an opportunity to assume that indium-enhanced fluorescence in the UV region is also likely to depend on irradiation power. Note: the results of the MEF-UV study here were obtained using low power ($\ll 2$ mW at 280 nm) excitation (see Sec. II). Subsequently, we speculate that applying higher power UV lasers can significantly increase the observed MEF effects and the further increased detectability of protein residues. Work in this regard is currently underway in our laboratory and the results will be reported in due course.

IV. CONCLUSIONS

The vacuum deposition of indium onto glass slides produces metal films of different thickness and morphology.

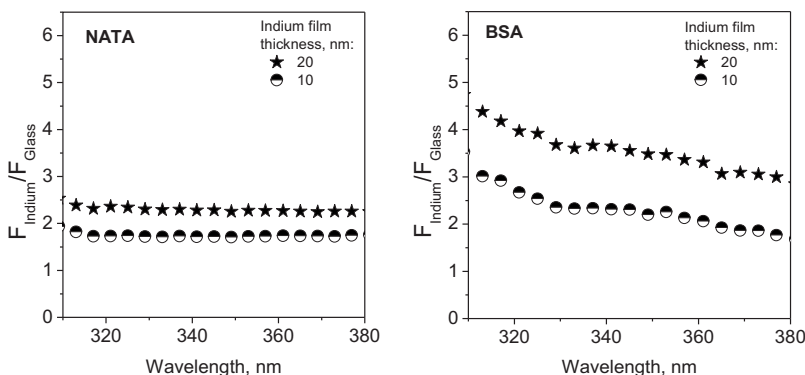


FIG. 9. Dependence of the MEF effect upon wavelength of fluorescence of NATA (left) and BSA (right), loaded onto indium slides of 10 and 20 nm thickness, as measured on the quartz crystal microbalance.

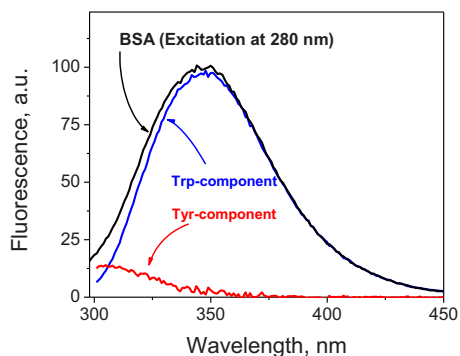


FIG. 10. (Color online) Deconvolution of the BSA fluorescence spectra into two emission components, Trp- and Tyr-components.

Analysis of the optical density spectra of indium slides has shown that there are three distinct morphological states of the indium coating: (a) random distribution of equal size NPs on a glass surface (low indium density, 2–6 nm thickness). The position of the plasmon resonance band does not change and MEF depends linearly with indium coating density; (b) an intermediate state, which one can characterize as a saturation of the surface with metal NPs, and the formation of a thin semicontinuous film (8–12 nm thickness). This state is characterized by a low MEF effect for UV fluorescence of Tyr and Trp, and a broad dispersion of plasmon frequencies over a broad spectral range; (c) and finally, the presence of large particles, possibly, located on the preformed continuous thin film (high indium density, >12 nm thickness). This hypothesis subsequently explains the significant change in plasmon resonance frequencies (shift nearly 150 nm to the red) and the progressive increase in MEF with indium film thickness.

Fluorescence enhancement of intrinsic protein chromophores (Tyr, Trp), follows the change in indium coating thickness, exhibiting a pronounced dependence on the metal landscape.

Fluorescence of the large globular protein, BSA, also significantly enhances on an indium substrate. The magnitude of the MEF enhancement is in the range of threefold to fivefold for low power irradiance. Remarkably in the case of BSA fluorescence, the MEF effect considerably depends on wavelength, showing an increase at shorter (<330 nm) wavelengths, which correlates with the position of the Tyr fluorescence maximum, whereas for NATA alone, the fluorescence enhancement is constant over the whole range of fluorescence emission. One can conclude that for proteins, the dependence of MEF upon wavelength could reflect the distribution of intrinsic chromophores (Tyr, Trp) within a protein globule and, consequently, the strength of interaction with the near-field, associated with surface plasmons.

The results of this study clearly show that indium is an effective substrate for MEF in the UV spectral region and

offers significant opportunities for the labelless detection of biomolecules. To the best of our knowledge this is the first report regarding indium plasmon coupling with intrinsic protein fluorescence in the MEF literature.¹³

ACKNOWLEDGMENTS

We thank the Department of Chemistry and Biochemistry, University of Maryland Baltimore County, and the Institute of Fluorescence for financial support and salary.

- ¹J. R. Lakowicz, *Principles of Fluorescence Spectroscopy*, 3rd ed. (Springer Science Business Media, New York, 2006).
- ²K. Aslan and C. D. Geddes, in *Metal-Enhanced Fluorescence*, edited by C. D. Geddes (Wiley, New York, 2010), p. 1.
- ³K. H. Drexhage, *J. Lumin.* **1**, 693 (1970).
- ⁴C. D. Geddes and J. R. Lakowicz, *J. Fluoresc.* **12**(2), 121 (2002).
- ⁵B. N. J. Persson, *J. Phys. C* **11**, 4251 (1978).
- ⁶C. D. Geddes, I. Gryczynski, J. Malicka, Z. Gryczynski, and J. R. Lakowicz, *Comb. Chem. High Throughput Screening* **6**(2), 109 (2003).
- ⁷C. D. Geddes, A. Parfenov, D. Roll, I. Gryczynski, J. Malicka, and J. R. Lakowicz, *J. Fluoresc.* **13**, 3 (2003).
- ⁸Y. Chen, K. Munechika, and D. S. Ginger, *Nano Lett.* **7**(3), 690 (2007).
- ⁹S. D'Agostino, P. P. Pompa, R. Chiuri, R. J. Phaneuf, D. G. Britti, R. Rinaldi, R. Cingolani, and F. Della Sala, *Opt. Lett.* **34**, 2381 (2009).
- ¹⁰J. Kim, G. Dantelle, A. Revaux, M. Berard, A. Huignard, T. Gacoin, and J. P. Boilot, *Langmuir* **26**, 11 (2010).
- ¹¹A. Renier, T. Mangeat, H. Benalia, C. Elie-Caille, C. Pieralli, and B. Wacogne, *Laser Phys.* **20**, 591 (2010).
- ¹²M. Staiano, E. G. Matveeva, M. Rossi, R. Crescenzo, Z. Gryczynski, I. Gryczynski, L. Iozzino, I. Akopova, and S. D'Auria, *Acs Applied Materials & Interfaces* **1**, 2909 (2009).
- ¹³C. D. Geddes, *Metal-Enhanced Fluorescence* (Wiley, New York, 2010).
- ¹⁴Y.-X. Zhang, A. Dragan, and C. D. Geddes, *J. Appl. Phys.* **107**, 024302 (2010).
- ¹⁵R. Pribik, K. Aslan, Y. X. Zhang, and C. D. Geddes, *J. Phys. Chem. C* **112**, 17969 (2008).
- ¹⁶Y. X. Zhang, A. Dragan, and C. D. Geddes, *J. Phys. Chem. C* **113**, 36 (2009).
- ¹⁷K. Aslan, M. J. R. Previte, Y. X. Zhang, and C. D. Geddes, *J. Phys. Chem. C* **112**, 47 (2008).
- ¹⁸Y. X. Zhang, K. Aslan, M. J. R. Previte, and C. D. Geddes, *Appl. Phys. Lett.* **90**, 173116 (2007).
- ¹⁹M. H. Chowdhury, K. Ray, S. K. Gray, J. Pond, and J. R. Lakowicz, *Anal. Chem.* **81**, 4 (2009).
- ²⁰E. A. Burstein, *Intrinsic Luminescence of Proteins* (VINITI, Academy of Science, Moscow, USSR, 1977).
- ²¹A. P. Demchenko, *Ultraviolet Spectroscopy of Proteins* (Springer-Verlag, New York, 1981).
- ²²R. Pribik, A. I. Dragan, Y. Zhang, C. Gaydos, and C. D. Geddes, *Chem. Phys. Lett.* **478**, 70 (2009).
- ²³E. A. Permyakov, *Luminescent Spectroscopy of Proteins* (CRC, London, 2010).
- ²⁴M. H. Chowdhury, K. Aslan, S. N. Malyn, J. R. Lakowicz, and C. D. Geddes, *Appl. Phys. Lett.* **88**, 173104 (2006).
- ²⁵Y. Zhang, A. Dragan, and C. D. Geddes, *J. Phys. Chem. C* **113**, 28 (2009).
- ²⁶C. Hilger, F. Grigioni, B. C. De, G. Michel, J. Freilinger, and F. Hentges, *Clin. Exp. Immunol.* **123**, 387 (2001).
- ²⁷C. Crane-Robinson, C. M. Read, P. D. Cary, P. C. Driscoll, A. I. Dragan, and P. L. Privalov, *J. Mol. Biol.* **281**, 4 (1998).
- ²⁸K. Ray, R. Badugu, and J. R. Lakowicz, *Chem. Mater.* **19**, 24 (2007).
- ²⁹R. L. Stoermer and C. D. Keating, *J. Am. Chem. Soc.* **128**, 13243 (2006).
- ³⁰A. I. Dragan and C. D. Geddes, "Excitation Volumetric Effects (EVE) in Metal-Enhanced Fluorescence," *Phys. Chem. Chem. Phys.* (to be published).